Presented at the WCPEC-8, 8th World Conference on Photovoltaic Energy Conversion, 26-30 September 2022, Milan, Italy

VIRTUAL ENERGY RATING: A METHOD FOR OPTIMIZING MODULE PERFORMANCE THROUGH CELL-TO-MODULE ANALYSIS

A. Protti, J. Shahid, M. Mittag, D. H. Neuhaus, U. Kräling, M. Kaiser
Fraunhofer Institute for Solar Energy Systems ISE
Heidenhofstr. 2, 79110 Freiburg, Germany
alexander.aguilar.protti@ise.fraunhofer.de

ABSTRACT: The implementation of energy rating of photovoltaic modules based on IEC-61853 imposes challenges to developers of PV module technology. In response, we present how a simulation-based analysis methodology, adapted for non-STC conditions, can be used to obtain all information needed for determining a virtual Climate Specific Energy Rating (vCSER), namely: a power matrix, the spectral response, the angular loss, and heat transfer coefficients. A conventional full-cell module and a "butterfly" half-cell topology are used to exemplify how the proposed method can be used to identify gain and loss factors of a module design affecting the performance of each module in terms of rated energy yield per area and Climate Specific Energy Rating (CSER). Recommendations for improving the module design are ranked and discussed, based on a sensitivity analysis on eleven parameters.
Keywords: Energy Rating, Simulation, PV Module, Design, Performance

1 INTRODUCTION

Photovoltaic (PV) modules are to some extend priced based on their rated power, measured at Standard Test Conditions (STC: 1000 W/m^2 irradiance, 25°C module temperature and AM1.5G spectrum [1]) which are rarely found at installation sites. However, environmental conditions and how a module responds to them defines the energy yield of a module and the economic revenue that can be obtained from it. As solar modules constitute one of the main cost of PV systems [2], improving the way in which modules are rated can foster innovation and the bankability of PV projects.

In response, the International Electrotechnical Commission (IEC) introduced the IEC 61853 series: Photovoltaic (PV) module performance testing and energy rating [3–6], which provides an international standard for the PV industry to characterize and compare modules based on an estimation of their performance for typical climatic regions, without the effect of the PV system (shading, inverter, AC cables, transformer, etc.) or module degradation.

As the IEC 61853 gains relevance in the PV market [7–11], module producers might adapt the design and the bill of materials (BOM) of their modules with focus on the energy rating. Nonetheless, various issues have been pointed out regarding the costs of the additional measurements needed for characterizing the modules [12] and the difficulties in achieving an unanimous interpretation and application of the standard [13,14]. In other words, the IEC 61853 implies additional challenges that might increase the time-to-market of new technologies and slow down the overall development of the PV industry.

To overcome this barrier, the current work presents how a cell-to-module (CTM) analysis model [15–17] extended for non-STC simulations [18] can be used to calculate a virtual Climate Specific Energy Rating (vCSER). This model, which requires as input the module layout and the physical properties of the module components, allows to reduce expenses from prototyping, field testing and the additional measurements required by the standard [3,4], during the development phase of a module. Furthermore, it enables a rapid assessment of the impact of module design parameters on its performance, facilitating the usage of the energy rating as a tool in technology development and benchmarking. It also allows to give a forecast or a quick update of the energy rating of a module for higher power cell classes.

A similar methodology has been implemented by Blakesley [12] for optimizing the costs of the CSER, however his analysis aims at minimizing the costs of the measurements needed for the IEC 61853 and the electrical losses in the module design are not explicitly contemplated in his model. Haedrich [19], Thomson [20] and Mittag [21] have also applied CTM analysis for yield simulations. However, their work does not follow the IEC 61853 procedure. Furthermore, Haedrich [19] and Thomson [20] make use of various independent models. In contrast, the current work has been implemented in a consistent bottom-up multi-physics loss channel analysis ("SmartCalc.Module") [22,23], whose graphical user interface facilitates the usage of the model for rapid assessment of module technology.

In the next section, the details of IEC 61853 relevant for explaining our approach are presented. Then, the vCSER approach and its application are shown. This paper finalizes with a summary of the main aspects that were discussed.

2 OVERVIEW OF THE ENERGY RATING BASED ON IEC 61853

The IEC 61853 series (from now on, "the standard", for simplicity) consists of four parts which establish the characterization methods [3,4], a reference weather data set [6] and the algorithm [5] for calculating the energy output of the module [Wh] for each time step and for a whole year (rated power or yield, $E_{mod,year}$ [$Wh/year$]):

$$E_{mod,year} = \sum_{j=1}^{j=8760} P_{mod,j} \cdot 1\ hour \qquad (1)$$

where $P_{mod,j}$ [Wp] is the module maximum power point at the given conditions for each timestep j. The standard also defines the Climate Specific Energy Rating (CSER, dimensionless), which corresponds to the annual performance ratio (PR) of the PV module for each climatic region:

$$CSER = \frac{E_{mod,year}/H_p}{P_{mpp,STC}/G_{ref}} \quad (2)$$

Here H_p [Wh/m^2] is the total of the hourly global in-plane irradiation for the reference period, G_{ref} is the irradiance at STC (1000 W/m^2), and $P_{mpp,STC}$ [Wp] the corresponding maximum power at STC.

2.1 Inputs for the IEC 61853 algorithm

The algorithm of the standard [5] requires four inputs: a power matrix, the spectral response, the angular dependence, and the thermal coefficients for calculating the module operating temperature. These inputs are sequentially used for obtaining discount coefficients associated to each environmental factor, which are then used to calculate the energy, generated by the module at each time step, given the weather data [6].

2.1.1 Power matrix (PM)

The PM accounts for the response of the module to light intensities and temperatures different from STC. It consists of a set of P_{MPP} values obtained from IV curve measurements at the temperatures and irradiances shown in Table I. The full matrix consists of 22 data points. The measurements can be done either outdoor or indoor. Details for the interpolation and extrapolation of the data are part of the algorithm [5].

Table I: Temperatures and irradiances needed for the power matrix according to IEC 61853

Irradiance [W/m^2]	Module temperature [$°C$]			
	15	25	50	75
100			NA	NA
200			NA	NA
400				NA
600				
800				
1000				
1000	NA			

2.1.2 Spectral response (SR)

The SR is used for obtaining the spectral mismatch of the module and for correcting to the reference spectral conditions during module characterization. It must be measured following the procedure from IEC 60904-8 [24].

2.1.3 Angular dependence

This input accounts for the changes in the module I_{SC} at 25 $°C$ with respect to the angle of incidence (θ). Hence, it is used to calculate the effective light transmission (τ) in the module at different incidence angles, which affects how the module responds to both direct and diffuse light. For simplicity of computation, a fitting of the measurements to the Martin-Ruiz model [25] is suggested by the standard, so that the measurements can be summarized by the angular loss coefficient (a_r, also known as the angle of incidence response [4]). The following equation applies:

$$\tau(\theta) = \frac{Isc(\theta)}{Isc(0)\,cos(\theta)} = \frac{1 - e^{\frac{-\cos(\theta)}{a_r}}}{1 - e^{\frac{-1}{a_r}}} \quad (3)$$

2.1.4 Coefficients for calculating the module operating temperature

These coefficients are obtained from fitting the Faiman model [26] to outdoor measurements. Here, the sample module and additional reference modules are required. The data used in the fitting must include measurements from at least ten different days which contain no less than ten valid points before and after noon. The valid data points must fulfill steady state requirements within irradiance and wind speed limits further detailed in the standard [4]. The model for relating the irradiance on the module (G [W/m^2]), the wind speed (v [m/s]), the module operating temperature (T_{mod}, °C) and the ambient temperature (T_{amb} [°C]) has the form:

$$\frac{G}{T_{mod} - T_{amb}} = u_0 + u_1 v \quad (4)$$

Here u_0 [W/m^2/°C] describes the influence of the irradiance at no-wind conditions and u_1 [W-s/m^3/°C] describes the wind impact.

2.1 Standard reference climatic profiles

The reference weather data set provided in the standard [6] contains tabulated data of hourly values over a full year for six different climatic profiles:

Table II: Locations and climatic profiles used in the IEC 61853

Latitude	Type
1°S	Tropical Humid
33°30'N	Subtropical arid (desert)
33°22'N	Subtropical coastal
56°N	Temperate coastal
34°N	High elevation (above 3000 m)
57°N	Temperate continental

The given weather variables are a time stamp, local solar time, ambient temperature, wind speed at the module height, solar angles, direct and global horizontal irradiance, direct and global in-plane irradiance, and spectrally resolved global in plane-irradiance for a set of discrete band intervals.

3 VIRTUAL ENERGY RATING MODEL

The calculation procedure consists of two stages. In the first stage, the model relies on a physical characterization of the individual module components to calculate all the inputs needed for the IEC 61853 algorithm by using a CTM model [15–17], which has been extended and validated for non-STC conditions as explained in [18]. At a second stage, the algorithm from the standard [5] is used to estimate the yield and a virtual CSER of the module. For ease of use, the model has been implemented in the software SmartCalc.Module [22,23], which can be downloaded from www.cell-to-module.com.

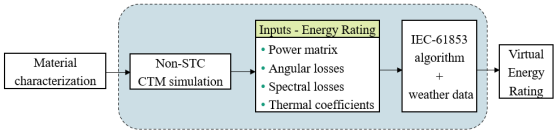

Figure 1: Flow diagram of the virtual Energy Rating

For calculating the power matrix, a linear behavior of the photo-current from the one-diode-model is assumed. Temperature coefficients for P_{MPP}, I_{SC} and V_{OC} are considered independent from the irradiance.

Fresnel equations as presented in [18] are used to make angularly and spectrally resolved calculations of the optical losses due to the module cover and encapsulants. With respect to the optical coupling, the gains from reflective back sheets can also calculated in detail as described by [17]. The optical coupling gains from cell metallization, interconnection ribbons and the cell-encapsulant coupling are considered as a constant value for all angles and wavelengths. This way, a synthetic value of the SR and a_r that responds to changes in the optical properties of the module is generated.

A one-dimensional thermodynamical model described by Mittag [27] is used to obtain the temperature under different operating conditions. A sample of the weather data from the standard [6] that fulfills the requirements from [4] is used as weather input for the calculations. Finally, u_0 and u_1 are obtained with the least-squares method. It is worth mentioning that the standard [4] warns about potentially large variation in the values of these coefficients, depending on the location and the season. In contrast, the proposed approach is less sensitive to these conditions because the data points selected are chosen using a pseudo-random sequence, which allows direct repeatability of the weather data.

4 APPLICATION OF THE VIRTUAL ENERGY RATING

To illustrate the application of the virtual energy rating procedure, two exemplary modules are considered. Module A is constituted by 60 M4 full square cells connected in series. Module B contains 120 half-cut cells connected in a "butterfly" topology (2 parallel blocks of 60 cells connected in series). The module layout follows the specifications presented in Table III. Here, the top margin is 10 *mm* less in module B because the string interconnector is placed between the two parallel blocks of cells. Hence, module B has 10 *mm* in its center, between both cell blocks. However, module B is 22.5 *mm* longer, because it has nine additional cell spaces along its length. The rest of the layout dimensions are the same for both module designs.

Table III: Module layout

Characteristic	Module A	Module B
String connection type	Series	Butterfly
Cells per string	10	10
Strings per module	6	12
Middle distance [*mm*]	0	10
Top margin [*mm*]	20	10
Bottom margin [*mm*]	10	10
Side margins [*mm*]	10	
Cell distance [*mm*]	2.5	
String distance [*mm*]	2.5	
Frame width [*mm*]	13	
Module length [*mm*]	1696	1718.5
Module width [*mm*]	1029	1029
Module area [m^2]	1.745	1.768

The IV curve characteristics of the cells, taken from [28], are shown in Table IV. Here, the cell cutting generates a reduction in cell efficiency of 0.32%$_{abs}$. However, since both cell types have practically the same efficiency, a clean comparison between module designs can be done.

Table IV: Cell specifications

Characteristic	Module A	Module B
Cell type	Full cells	Half cells with edge losses
Length [mm]	161.75	80.875
Width [mm]	161.75	161.75
Pseudo-square diameter [mm]	0	0
Area [cm^2]	261.631	130.815
Number of busbars	6	6
I_{SC} [A]	10.46	5.23
V_{OC} [V]	0.683	0.681
I_{MPP} [A]	10.00	4.97
V_{MPP} [V]	0.585	0.580
P_{MPP} [Wp]	5.85	2.88
Fill factor [%]	81.88 %	80.93 %
Efficiency	22.36%	22.04 %
Metallized area (front) [mm^2]	888	444

4.1 Comparison of module designs

4.1.1 CTM analysis

The cell to module analysis is shown in Figures 2 and 3. With respect to the efficiency, the module margin (k1) and cell spacing (k2) are the main cause of efficiency loss in both modules. The additional cell spaces of module B contribute to increasing the total active area loss (k1+k2) by 0.24%$_{abs}$ with respect to module A, which also leads module B to having 0.06%$_{abs}$ greater cover coupling gains (k11). As a result, the geometrical and optical losses in module B are 0.18%$_{abs}$ greater than in module A.

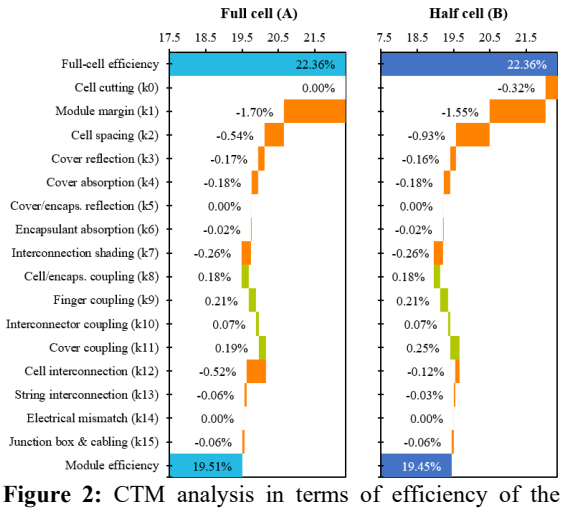

Figure 2: CTM analysis in terms of efficiency of the module design with full cells (A) and half cells (B)

With respect to the electrical factors, module B has about four times less efficiency losses in the cell interconnectors (k12) because half as much current flows through them ($\Delta P=I^2*R$). Also, half of the current flows through about two thirds of the string interconnector length, leading module B to having half the losses in these elements (k13). The resulting advantage of 0.43%$_{abs}$ less electrical losses (k12-k15) is 0.25%$_{abs}$ greater than the

difference in the optical factors. However, it is not enough to overcome the 0.32%$_{abs}$ losses due to cell cutting, leading the butterfly topology (module B) to have and efficiency of 19.45%, which is 0.06 %$_{abs}$ or 3%$_{rel}$ smaller than module A (19.51% efficiency).

Regarding the CTM in terms of module power (Figure 3), the inactive area only plays a role in the optical gains (k11), but not in the losses. Therefore, module B has a rated power of 343.88 *Wp*, which is greater than the 340.57 *Wp* of module A by a difference of 3.31 *Wp* (less than 1%).

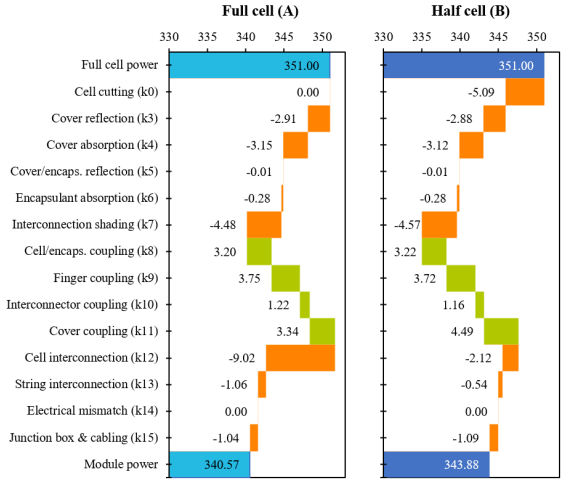

Figure 3: CTM analysis in terms of power of the module design with full cells (A) and half cells (B)

4.1.2 Results from the virtual Energy Rating

When looking at the results from the virtual Energy Rating (Figures 4 and 5) module A has an advantage over module B for all climatic regions. In terms of yield per area and vCSER, module A is on average 1.19% and 1.44% better than module B.

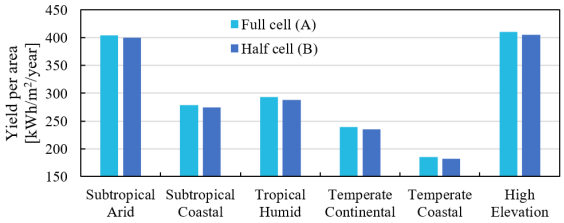

Figure 4: Energy yield per area of module A and module B for six climatic regions

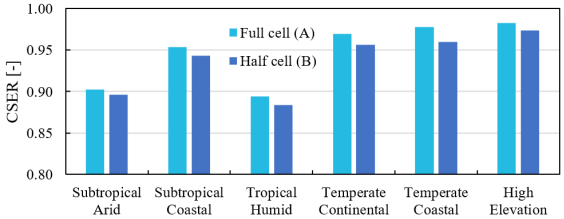

Figure 5: Virtual Climate Specific Energy Rating of module A and module B for six climatic regions

With respect to the causes for these results, Figures 6 and 7 show that half-cut cells module has a worse low light response [28], which it a competitive disadvantage with respect to the simulated full cell module when partial shading at the installation site is not expected [29].

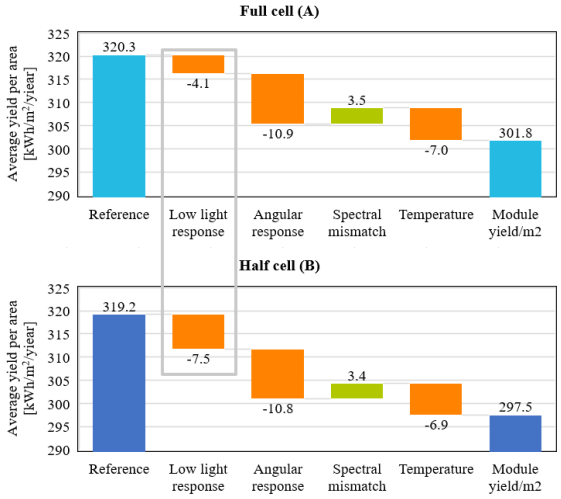

Figure 6: Comparison of environmental factors affecting the CSER of module A and B

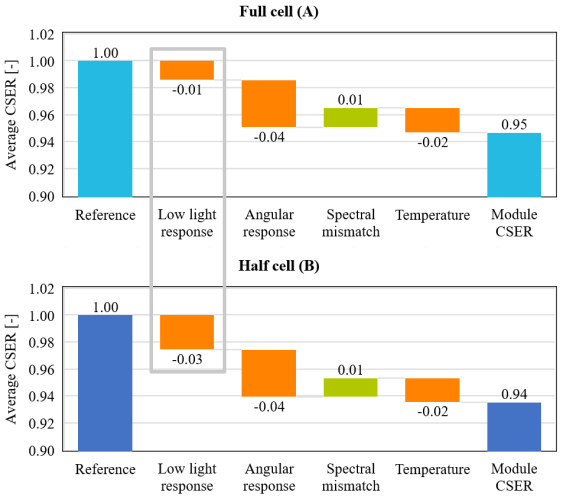

Figure 7: Comparison of environmental factors affecting the average yield per area of module A and B

4.2 Sensitivity analysis on module design parameters

We now illustrate how the energy rating of module B could be improved by changing its design. For narrowing the analysis, a selection of eleven parameters is done based on the CTM analysis. The results are presented in Figure 8 and Figure 9 in the form of spider plots. For comparison, the changes are expressed as percentual change with respect to the initial reference value.

Regarding the yield per area, increasing the number of strings per module has the most important effect, followed by the number of cells per string. When changing these parameters, it is assumed that spacings and margins are kept the same, but more cells or strings are added (or removed), meaning that the number of cells and module dimensions are increased (decreased). In principle, adding either cells or strings improve in a similar way the active area share. However, having more cells in a string would also increment the cell interconnection losses (k12), whereas the strings per module couple with the string connector losses, which are lower due to the larger cross section of the string connector ribbon.

Next in line, comes increasing the thickness of the cell and string interconnector. These actions would not have a direct impact on any other variable, than themselves and the downstream electrical losses.

Increasing the width of the string interconnector has an equivalent effect to increasing its thickness, since both improve its cross-section area and reduce its resistance. The sensitivity for these two parameters is clearly non-linear because the dependency between solar cells and the series resistance follows the diode model and because the irradiance distribution is skewed towards low light conditions, giving a lower marginal benefit to having lower resistance at higher irradiance conditions.

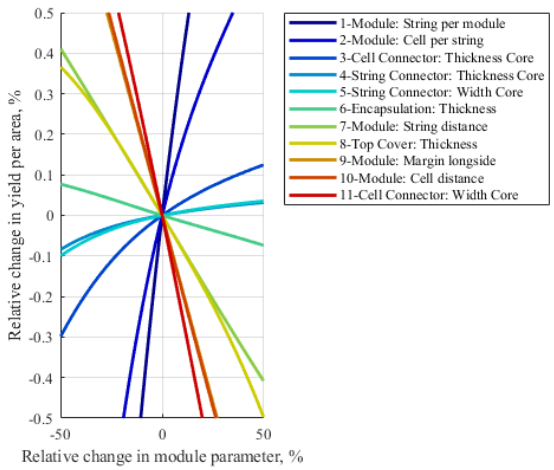

Figure 8: Spider plot depicting the sensitivity of the yield per area of module B with respect to module design parameters

The small negative effect of increasing the thickness of the encapsulant means that this parameter could be adjusted if having thicker interconnectors caused problems in the lamination process.

Then, reducing the string distance would increase the module packing density and decrease the total module area. This would also shorten the string connectors. A similar effect on the yield per area is observed when the glass thickness is reduced.

Following, a reduction in the module margin and the cell distance would reduce the module area, improving the yield per area. Here, a decrease in the losses due to the cell connectors when reducing the cell distance, gives this aspect a greater impact.

Finally, the shading caused by the cell connector could be reduced by making it narrower. Any increments on the resistance, are less important.

Before looking at the results from the sensitivity analysis on the CSER, it is worth noticing that a module designed by CSER optimization is different from a module optimized for yield per area, because the area units in the definition of the CSER (Equation 2) are cancelled out. In other words, the CSER can be understood as a normalized ratio between rated yield and rated power (G_{ref} and H_p are constant).

Consequently, in Figure 9, we observe that increasing the module margin, string distance and cell distance has a positive impact on the CSER, because that would increment the gains from the internal light recycling, the back cover coupling (k11).

Also, we see that the cell interconnector width result has a U-shape, being the current width close to the minimum CSER. In other words, a different width will improve the yield to power ratio.

In the case of the string interconnector, increasing either its width or thickness will also have a negative effect on the CSER, since the benefits on the rated power are lower compared to the yield gains. Nonetheless, a reduction in the encapsulation or in the front cover thickness would have a beneficial impact on the yield to power ratio.

In the case of the cells per string and the strings per module, the associated losses from the interconnectors have a negative impact on the CSER.

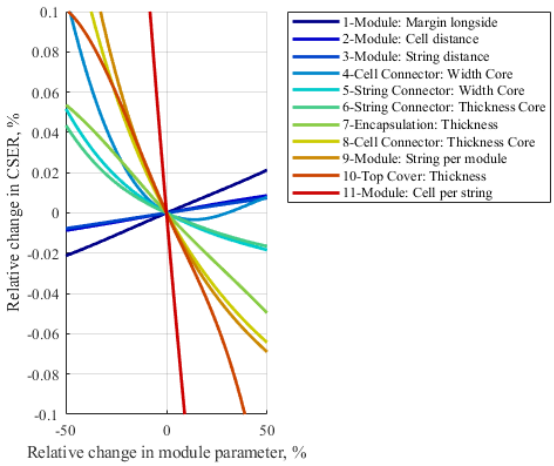

Figure 9: Spider plot depicting the sensitivity of the CSER of module B with respect to module design parameters

Finally, the effect on the yield per area of improving five selected parameters by 20% in the design of module B can be observed in Figure 10. The yield per area of the changed design is 301.8 W/m^2/year, which is 1.45% better than the initial design and is now as good as the reference full cell module. Regarding the rated efficiency and rated power at STC, they are now 19,74% and 345,0 Wp, respectively, which are both better than the reference values of both modules.

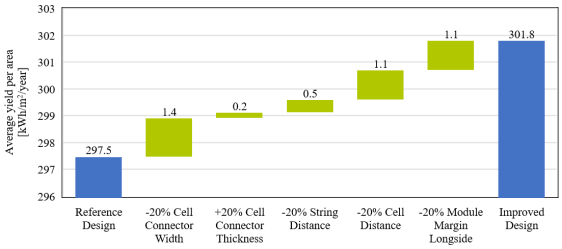

Figure 10: Gains in the average yield per area from sequential changes in the design of module B

4 CONCLUSIONS

A methodology for studying and quantifying the effect of module design parameters on the rated yield of a PV module, using Cell-to-Module simulations and the algorithm from the IEC 61853, is presented. It is also shown how the vCSER can be used for relating the rated power with the rated yield of a module.

It is expected that the vCSER approach assists module manufacturers in their decision making and speeds up the development of photovoltaic modules with an improved performance, by reducing the need for prototyping and testing specially in the early stages of product development.

6 AKOWLEDGEMENT

We would like to thank the German Federal Ministry for Economic Affairs and Climate Action (FKZ 0324289 and 03EE1028) for its funding.

7 REFERENCES

[1] International Electrotechnical Commission, Photovoltaic devices – Part 1: Measurement of photovoltaic current-voltage characteristics, 3rd ed., International Electrotechnical Commission (IEC), Geneva, Switzerland, 2020.

[2] IRENA, Renewable Power Generation Costs in 2020 (2021).

[3] International Electrotechnical Commission, Photovoltaic (PV) module performance testing and energy rating – Part 1: Irradiance and temperature performance measurements and power rating, 1st ed., IEC Central Office, Geneva, Switzerland, 2011.

[4] International Electrotechnical Comission, Photovoltaic (PV) module performance testing and energy rating – Part 2: Spectral responsivity, incidence angle and module operating temperature measurements, 1st ed., IEC Central Office, Geneva, Switzerland, 2016.

[5] International Electrotechnical Commission, Photovoltaic (PV) module performance testing and energy rating – Part 3: Energy rating of PV modules, 1st ed., IEC Central Office, Geneva, Switzerland, 2018.

[6] International Electrotechnical Commission, Photovoltaic (PV) module performance testing and energy rating – Part 4: Standard reference climatic profiles, 1st ed., IEC Central Office, Geneva, Switzerland, 2018.

[7] N. Dodd, N. Espinosa, Preparatory study for solar photovoltaic modules, inverters and systems, 2019.

[8] A. Wade, et al., The Product Environmental Footprint (PEF) of photovoltaic modules-Lessons learned from the environmental footprint pilot phase on the way to a single market for green products in the European Union, Prog Photovolt Res Appl 26 (2018) 553–564. https://doi.org/10.1002/pip.2956.

[9] D. Polverini, et al., Building Criteria for Energy Labeling of Photovoltaic Modules and Small Systems, Solar RRL 6 (2022) 2100518. https://doi.org/10.1002/solr.202100518.

[10] European Commission. Joint Research Centre., Preparatory study for solar photovoltaic modules, inverters and systems: final report, Publications Office, 2020.

[11] A. Wade, et al., The Product Environmental Footprint (PEF) of photovoltaic modules-Lessons learned from the environmental footprint pilot phase on the way to a single market for green products in the European Union, 2021.

[12] J.C. Blakesley, et al., Accuracy, cost and sensitivity analysis of PV energy rating, Progress in Solar Energy 1 203 (2020) 91–100. https://doi.org/10.1016/j.solener.2020.03.088.

[13] N. Riedel-Lyngskær, et al., Interlaboratory comparison of angular-dependent photovoltaic device measurements: Results and impact on energy rating, Prog. Photovolt: Res. Appl. 29 (2021) 315–333. https://doi.org/10.1002/pip.3365.

[14] M.R. Vogt, et al., Interlaboratory Comparison of the PV Module Energy Rating Standard IEC 61853-3. 5 pages / 37th European Photovoltaic Solar Energy Conference and Exhibition; 811-815 (2020). https://doi.org/10.4229/EUPVSEC20202020-4BO.13.2.

[15] I. Hädrich, et al., Unified methodology for determining CTM ratios: Systematic prediction of module power, Sol Energ Mat Sol C 131 (2014) 14–23. https://doi.org/10.1016/j.solmat.2014.06.025.

[16] M. Mittag, et al., Electrical and thermal modeling of junction boxes, in: Proceedings of the 33rd European Photovoltaic Solar Energy Conference and Exhibition (EU PVSEC), Amsterdam, Netherlands, 2017, pp. 1501–1506.

[17] A. Pfreundt, et al., Rapid Calculation of the Backsheet Coupling Gain Using Ray Groups, in: 35th European Photovoltaic Solar Energy.

[18] A. Pfreundt, M. Mittag, J. Shahid, Cell-To-Module Analysis Beyond Standard Test Conditions, in: 47th IEEE Photovoltaic Specialists Conference 2020.

[19] I. Haedrich, D.C. Jordan, M. Ernst, Methodology to predict annual yield losses and gains caused by solar module design and materials under field exposure, Solar Energy Materials and Solar Cells 202 (2019) 110069. https://doi.org/10.1016/j.solmat.2019.110069.

[20] A. Thomson, et al., Impact of PV module configuration on energy yield under realistic conditions, Opt Quant Electron 49 (2017) 329. https://doi.org/10.1007/s11082-017-0903-0.

[21] M. Mittag, et al., Approach for a Holistic Optimization from Wafer to PV System, in: Proceedings of the 7th World Conference on Photovoltaic Energy Conversion, Hawaii, 2018.

[22] Fraunhofer Institute for Solar Energy Systems ISE, SmartCalc.Module. http://www.cell-to-module.com (accessed 1 September 2022).

[23] M. Mittag, M. Ebert, Systematic PV module optimization with the cell-to-module (CTM) analysis software, Photovoltaics International (2017) 97–104.

[24] International Electrotechnical Commission, Photovoltaic Devices - Part 8: Measurement of Spectral Response of a Photovoltaic (PV) Device, International Electrotechnical Commission (IEC), Geneva, Switzerland, 1998.

[25] N. Martín, J.M. Ruiz, A new model for PV modules angular losses under field conditions, International Journal of Solar Energy 22 (2002) 19–31. https://doi.org/10.1080/01425910212852.

[26] D. Faiman, Assessing the outdoor operating temperature of photovoltaic modules, Prog. Photovolt: Res. Appl. 16 (2008) 307–315. https://doi.org/10.1002/pip.813.

[27] M. Mittag, et al., Thermal Modelling of Photovoltaic Modules in Operation and Production, in: 36th European Photovoltaic Solar Energy Conference and Exhibition (EUPVSEC) 2019.

[28] M. Mittag, et al., Techno-Economic Analysis of Half Cell Modules - The Impact of Half Cells on Module Power and Costs, 2019.

[29] N. Klasen, et al., A Comprehensive Study of Module Layouts for Silicon Solar Cells under Partial Shading, IEEE Journal of Photovoltaics (2022). https://doi.org/10.1109/JPHOTOV.2022.3144635.